PHYSICAL REVIEW B **78**, 125411 (2008)

Charge noise in single-electron transistors and charge qubits may be caused by metallic grains

S. Kafanov,[1,*] H. Brenning,[1] T. Duty,[1,2] and P. Delsing[1]
[1]*Microtechnology and Nanoscience, Chalmers University of Technology, S-41296, Göteborg, Sweden*
[2]*School of Physical Sciences, University of Queensland, St. Lucia, Queensland 4072, Australia*
(Received 14 April 2008; revised manuscript received 13 July 2008; published 17 September 2008)

We report on measurements of low-frequency noise in a single-electron transistor (SET) from a few hertz up to 10 MHz. Measurements were done for different bias and gate voltages, which allow us to separate noise contributions from different noise sources. We find a $1/f$ noise spectrum with two Lorentzians superimposed. The cut-off frequency of one of the Lorentzians varies systematically with the potential of the SET island. Our data is consistent with two single-charge fluctuators situated close to the tunnel barrier. We suggest that these are due to random charging of aluminum grains, each acting as a single-electron box with tunnel coupling to one of the leads and capacitively coupled to the SET island. We are able to fit the data to our model and extract parameters for the fluctuators.

DOI: 10.1103/PhysRevB.78.125411 PACS number(s): 07.20.Mc, 73.23.Hk

I. INTRODUCTION

Single-electron transistors (SETs)[1,2] are extremely sensitive electrometers with demonstrated charge sensitivities of the order of $\mu e/\sqrt{\text{Hz}}$.[3,4] Due to their high-charge sensitivities, they have found a large number of applications in research, for example, SETs are used to detect nanomechanical oscillators,[5] to count electrons,[6,7] and to read out qubits.[8–10]

The fundamental limitation for the sensitivity of the SET is set by shot noise generated when electrons tunnel across the tunnel barriers.[11,12] Shot noise was observed in a two-junction structure (without gate) by Birk *et al.*[13]

However, there are two other types of noise, which is limiting the charge sensitivity in experiments. At high frequencies, above 1 MHz, the sensitivity is limited by amplifier noise. At low frequencies, the sensitivity is limited by $1/f$ noise, which is due to background charge fluctuators near the SET. A collection of several fluctuators with different frequencies leads to a $1/f$ spectrum. In several cases it has been observed that there is a background of $1/f$ noise and a single or a few more strongly coupled fluctuators resulting in random telegraph noise, which in the frequency spectrum, leads to Lorentzians superimposed on the $1/f$ background.[14,15]

Understanding the nature of the $1/f$ noise is also very important for solid-state qubits since $1/f$ noise strongly limits the decoherence time for these qubits. It has been suggested by Ithier *et al.*[16] that the charge noise has a cutoff at the frequency of the order of 0.5 MHz.

Even though there have been many efforts[14,15,17–24] to reveal the physical origin of the background charge fluctuators, the nature of these fluctuators is still unknown. It is not even clear where these fluctuators are located. The charge fluctuators can be located either in the tunnel barrier or outside the barrier but in close proximity of the junction.

The role of the substrate has been examined in several experiments.[17,19,25] However, those experiments did not show a strong dependence of the noise in the substrate material. The barrier dielectric has been proposed as location of the charge traps by several groups.[14,19,22,26]

Several groups have shown that the low-frequency noise at the output of the SET varies with the current gain $(\partial I/\partial Q_g)$ of the SET and that the maximum noise is found at the bias point with maximum gain.[20–22] This indicates that the noise sources acts at the input of the device, i.e., as an external fluctuating charge. A detailed comparison of the noise to the gain was done by Starmark *et al.*[20] All the above mentioned experiments were performed with conventional SETs by measuring current or voltage noises at relatively low frequencies, i.e., below a few kilohertz.

In this work we have measured low-frequency noise in a SET, which has demonstrated a very high-charge sensitivity,[4] by using the radio frequency-SET (rf-SET) technique.[27,28] This allowed us to measure low-frequency noise of the reflected voltage from the rf SET in the range of a few hertz up to tens of megahertz and, due to high-charge sensitivity, we were not limited by the amplifier noise. We find two Lorentzians superimposed on a $1/f$ spectrum and that the noise in the range 50 kHz–1 MHz is quite different for positive and for negative gains of the transistor. By analyzing the bias and gate dependence of the noise, we argue that the noise in this frequency range is dominated by electron tunneling to an aluminum grain, which acts as a single-electron box capacitively connected to the SET island.

The paper is organized as follows. In Sec. II we describe a model for the low-frequency noise, which allows us to separate contributions from the different noise sources. In Sec. III we describe the experimental details of our measurements. Section IV is the main part of this paper and contains the experimental results. Finally in Sec. V we describe our model for the nature of the low-frequency noise in our SETs.

II. LOW-FREQUENCY NOISE MODEL

We start by analyzing the different contributions of the measured noise. What we actually measure is the reflected voltage from the tank circuit in which the SET is embedded. The rf-SET tank circuit is a series LC circuit with inductance L and capacitance C. The power spectral density of the reflected voltage can be decomposed into the following terms originating from charge, resistance, shot, and amplifier noises according to the following equation:[20,29]

$$S_{|v_r|} = \left(\frac{\partial|v_r|}{\partial Q_g}\right)^2 S_{Q_g}(f) + \left(\frac{\partial|v_r|}{\partial R_1}\right)^2 S_{R_1}(f) + \left(\frac{\partial|v_r|}{\partial R_2}\right)^2 S_{R_2}(f) + S_{\text{Shot}} + S_{\text{Ampl.}}, \quad (1)$$

where Q_g is the charge at the input gate and $R_{1,2}$ are the tunnel resistances of the two junctions. Here we neglected the higher-order and possible correlation terms between the charge and the resistance noises. In the case when the charge fluctuator is located in the tunnel barrier, the correlation term may not be negligible. By measuring the noise for different bias points having different gains (i.e., different $\partial|v_r|/\partial Q_g$), it is possible to extract information on whether the noise is associated to charge or resistance fluctuators.

We have designed the matching circuit for the rf SET to work in the over-coupled regime, in order to have a monotonic dependence of the reflection coefficient as a function of the SET differential conductance. This regime corresponds to the matching condition when the internal quality factor of the rf-SET tank circuit ($Q_{\text{int}}=R/\sqrt{L/C}$) is larger than the external quality factor ($Q_{\text{ext}}=\sqrt{L/C}/Z_0$) where $Z_0=50\ \Omega$ is the characteristic impedance of the transmission line and R is the SET differential resistance.

We have theoretically analyzed the reflected voltage from the rf SET as a function bias and gate voltages applied to the SET. The reflected voltage characteristic of the rf SET can be calculated by the orthodox theory[30] using a master-equation approach. From this theory, we can also calculate the derivatives in Eq. (1) of the reflected voltage with respect to variations in gate charge and in the resistances of the SET tunnel junctions.

Figure 1(a) shows the sensitivity of the rf SET to charge fluctuations as a function of the bias and gate voltages. The charge sensitivity is a symmetric function around the SET open state ($Q_g=0.5e$) and has maxima close to the onset of the open state.

The sensitivity of the SET to resistance fluctuations in the first tunnel barrier is shown in Fig. 1(b). The sensitivity to resistance fluctuations in the second barrier (not shown) is identical to Fig. 1(b), except that it is mirrored along the SET open state ($Q_g=0.5e$).

By operating at different bias and gate voltages, we can choose operation points where the noise contribution from the different derivatives dominates and it is possible to distinguish charge noise from resistance noise.

III. EXPERIMENT DETAILS

The samples were fabricated on oxidized silicon substrates using electron-beam lithography and a standard double-angle evaporation techniques. The asymptotic resistance of the measured SET was 25 kΩ. The charging energy $E_C=e^2/2C_\Sigma \simeq 18\pm 2$ K was extracted from the measurements of the SET stability diagram of the reflected signal with frequency $f=350$ MHz versus bias and gate voltages. From the asymmetry of the SET stability diagram, we could also deduce that the asymmetry in the junction capacitances was 30%.

The SET was embedded in a resonant circuit and operated in the radio frequency mode.[27,28] The bandwidth of the setup

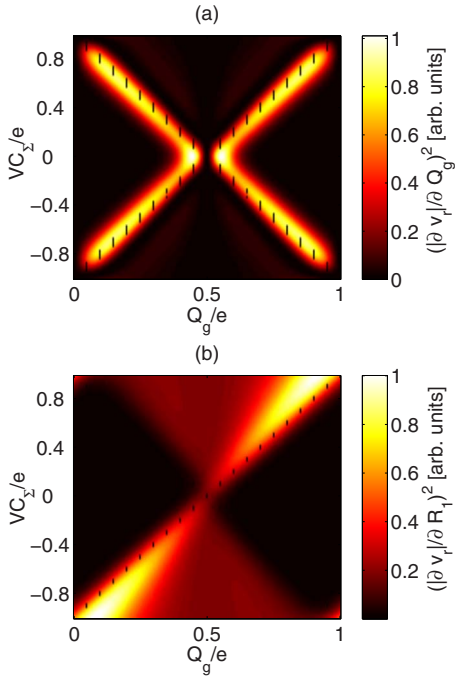

FIG. 1. (Color online) Calculated derivatives from Eq. (1) as a function of bias voltage V and gate charge $Q_g=C_gV_g$. The derivative of the reflected voltage from the rf SET with respect to (a) the charge fluctuations $(\partial|v_r|/\partial Q_g)^2$ and (b) the resistance fluctuations in the first junction $(\partial|v_r|/\partial R_1)^2$. Sensitivity to the resistance fluctuations in the second junction has a mirror symmetry, along SET open state ($Q_g=0.5e$), with the sensitivity to the resistance fluctuations in the first barrier.

was approximately 10 MHz limited by the quality factor of the resonance circuit. The radio frequency signal was launched toward the resonance circuit and the reflected signal was amplified by two cold amplifiers and then downconverted using homodyne mixing. The output signal from the mixer containing the noise information was then measured by a spectrum analyzer. The sample was attached to the mixing chamber of a dilution refrigerator, which was cooled to a temperature of approximately 25 mK. All measurements were performed in the normal (nonsuperconducting) state at a magnetic field of 1.5 T.

We have performed the noise measurements for different gate and bias voltages. Due to experimental problems, we have performed measurements mostly for negative biases. The sample shows very high-charge sensitivity of the order of 1 $\mu e/\sqrt{\text{Hz}}$. For a detailed description of the sensitivity with respect to different parameters see Ref. 4. A small sinusoidal charge signal of $7.3\cdot 10^{-4}$ e_{rms} with a frequency of 133 Hz was applied to the gate, which allowed us to calibrate the charge sensitivity referred to the input of the SET.

Before each measured spectrum, we have employed a charge-locked loop[31] with a help of a lock-in amplifier. The first $(\partial I/\partial Q_g)$ or the second $(\partial^2 I/\partial Q_g^2)$ derivatives of the current were used as an error signals for stabilization of the gate point to compensate for the slow drift at the current maximum points [**C** in Fig. 2(b)], or at the maximum gain points [**B** and **D** in Fig. 2(b)], respectively. Each noise spectrum is however measured with the feedback loop turned off.

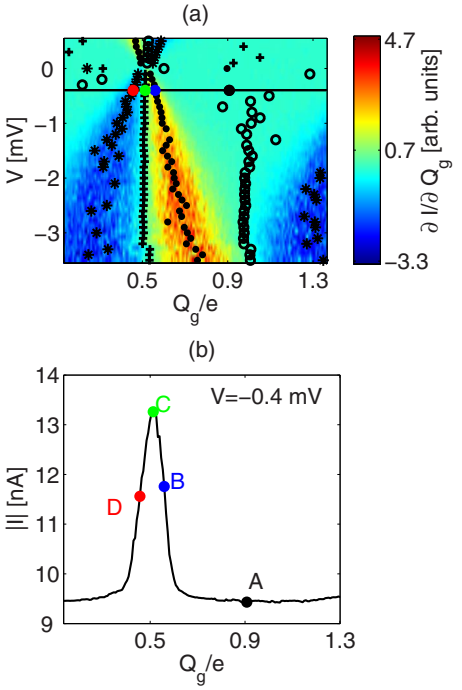

FIG. 2. (Color online) (a) The SET stability diagram $(\partial I/\partial Q_g)$ measured at a temperature of 25 mK. Horizontal black line corresponds to the bias voltage where transfer function $I(Q_g)$ [see panel (b)] was obtained. The points **A**/ ((◦) for negative and (+) for positive bias) where $I=0$ inside the Coulomb blockade region. The points **B** and **D** (∗/•) correspond to maximum positive/negative gains $\partial I/\partial Q_g$, that is, where $\partial^2 I/\partial Q_g^2=0$. The measurement points **C**, close to the current maximum current, correspond to $\partial I/\partial Q_g=0$ marked with (+) at negative bias and with (◦) at positive bias. (b) SET transfer function $I(Q_g)$ measured for the bias voltage $V=-0.4$ mV. In the stability diagram this measurement is shown as a black line.

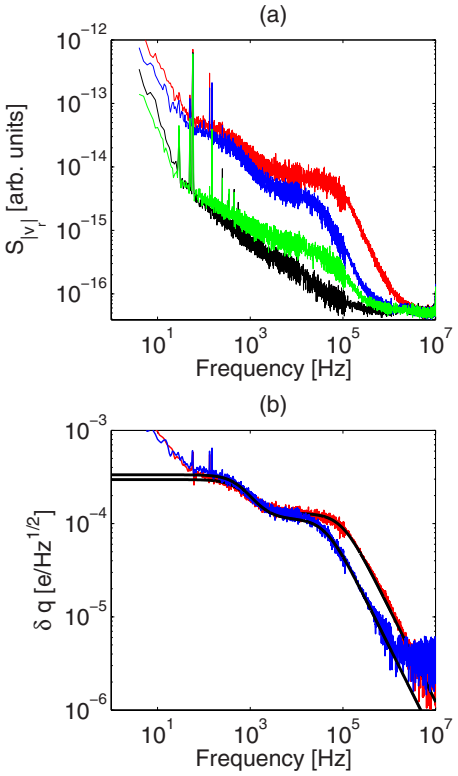

FIG. 3. (Color online) (a) Power spectral density (PSD) of the reflected voltage measured in the points **A** (black curve); **B** (blue curve); **C** (green curve); and **D** (red curve). (b) Normalized noise in the points **B** (blue curve) and **D** (red curve). The black continuous lines are fits to the measured PSD with a sum of two Lorentzian functions.

IV. EXPERIMENTAL RESULTS

In order to separate the contributions from different noise sources, we have performed measurements at specific points. The measurement points are shown in Fig. 2. At point **A** $(Q_g \approx 0e)$, there is an almost complete Coulomb blockade with a zero current and a zero gain $(\partial|v_r|/\partial Q_g=0)$. Here the derivatives of the reflected voltage with respect to resistance fluctuations in the tunnel barriers $(\partial|v_r|/\partial R_{1,2}=0)$ are also zero [see Fig. 1(b)]. At this point we see only amplifier noise, different curves for different bias voltages show the same noise level convincing us that we see only amplifier noise. These measurements thus serve to calibrate the noise of the amplifier.

The measurements at points **B** and **D** correspond to the requirement of maximum current gain $(\max|\partial I/\partial Q_g|)$ and therefore also high $|\partial|v_r|/\partial Q_g|$ [diagonals in Fig. 1(a)]. At these points there are contributions from all the noise sources (see Fig. 1), but since the absolute gain and the current are very similar at the points **B** and **D**, these measurements can be compared.

We have also measured noise at the points **C** $(Q_g \approx 0.5e)$ close to the maximum of the current transfer function $|(I(Q_g))|$. At this point the gain of the reflected signal $(\partial|v_r|/\partial Q_g)$ is quite low but the shot noise could be high. The derivatives of the reflected voltage with respect to resistance fluctuations in the tunnel barriers $(\partial|v_r|/\partial R_{1,2})$ are small but not equal to zero [see Fig. 1(b)].

The noise of the reflected voltage at the fixed bias point and for the different gate points are shown in Fig. 3(a). We start by subtracting the amplifier noise and then we compare the noise measured at the different points. Comparing the noise measured at points **B** and **D** where the current gain has a maximum, with the noise measured at point **C** close to the maximum of the transfer function, we see that the noise at the point **C** is substantially lower even though the current is higher. From this we draw the conclusion that the difference is not due to the shot noise.

Comparing the noise spectra measured at the points **B** and **D** (Fig. 3(b)), it is necessary to note that both the currents and the gains are very similar at these points. Both spectra **B** and **D** have a $1/f$ dependence at low frequencies with two Lorentzian shoulders at higher frequencies. At frequencies above 30 kHz, the noise at point **D** drops well bellow the noise at point **B**. At 300 kHz the difference is a factor of 5.

We have fitted the noise spectra at points **B** and **D** to a sum of two Lorentzian functions. The results of these fits are shown in Fig. 3(b). From these fits we can extract the cut-off frequency and the level for each of the two Lorentzians.

The low-frequency Lorentzian has a cut-off frequency of the order of 1 kHz. The cut-off frequency is the same for

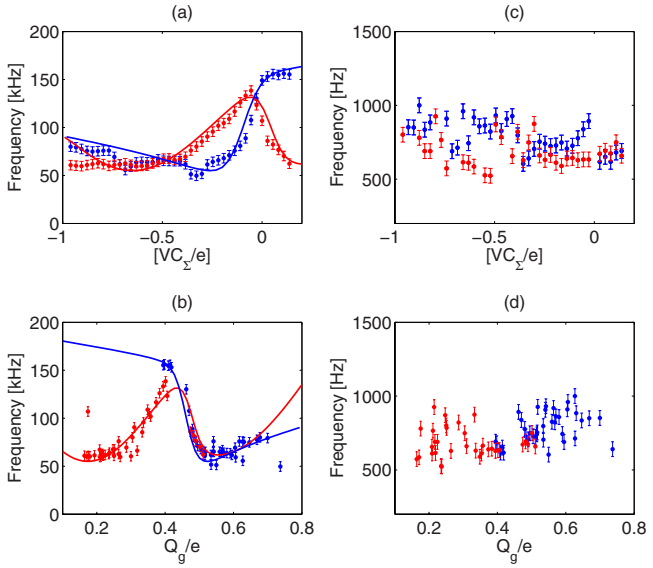

FIG. 4. (Color online) (a) Bias dependence of the cut-off frequency for the high-frequency Lorentzian. (b) Gate dependence of the cut-off frequency for the high-frequency Lorentzian. (c) Bias dependence of the cut-off frequency for the low-frequency Lorentzian. (d) Gate dependence of the cut-off frequency for the low-frequency Lorentzian. Blue points correspond to the negative slope $\partial I/\partial Q_g > 0$ (see Fig. 2). Red points correspond to the positive slope $\partial I/\partial Q_g < 0$ (see Fig. 2). The error bars are extracted from the fits to the Lorentzians. The continuous lines (blue and red) show the bias and gate dependencies for the Lorentzian cut-off frequency calculated in the described model.

both slopes ($\partial I/\partial Q_g \gtrless 0$) and it does not show any bias or gate dependence within the accuracy of our measurements.

In contrast, the high-frequency Lorentzian has a cut-off frequency above $f_{co} > 50$ kHz with a strong dependence on the bias and gate voltages. The bias dependence of the Lorentzian cut-off frequency for the positive ($\partial I/\partial Q_g > 0$) and negative ($\partial I/\partial Q_g < 0$) slopes are shown in Fig. 4(a).

For the negative slope ($\partial I/\partial Q_g < 0$) [blue points in Fig. 4(a)], the cut-off frequency remains practically constant ($f_{co} \simeq 50$ kHz) for negative biases. Close to the zero-bias voltage, the Lorentzian cut-off frequency switches to a higher frequency ($f_{co} \simeq 150$ kHz). For the positive slope ($\partial I/\partial Q_g > 0$) (red curve in Fig. 4), the situation is different. For negative-bias voltage, the Lorentzian cut-off frequency is continuously growing from $f_{co} \simeq 60$ kHz and reaches a maximum ($f_{co} \simeq 120$ kHz) close to zero-bias voltage. For the positive-bias voltage, it rapidly decreases from the maximum to the initial value $f_{co} \simeq 60$ kHz. Figure 4(b) shows the gate dependence for the Lorentzian cut-off frequencies for both slopes ($\partial I/\partial Q_g \gtrless 0$). As is clearly shown in this figure, the gate dependence for the positive and negative slopes are different. The gate dependence for the positive slope ($\partial I/\partial Q_g > 0$) (red curve) has a peak with a small negative offset on the gate charge from the SET open state. The Lorentzian cut-off frequency behavior on the negative slope ($\partial I/\partial Q_g < 0$) (blue curve) is a steplike function.

By integrating the Lorentzians in the noise spectra [see Fig. 3(b)], we can calculate the total variation of induced charge on the SET island for both fluctuators. The variation of induced charge, for the low-frequency fluctuator, is of the order of $\Delta q_{lf} \approx 6.6$ me$_{rms}$. The same estimation for the high-frequency fluctuator gives $\Delta q_{hf} \approx 30$ me$_{rms}$.

V. DISCUSSION

In this section we analyze the bias and the gate dependence of the cut-off frequency of the high-frequency Lorentzian ($f_{co} \simeq 50-150$ kHz). In particular, we try to explain why the cut-off frequency is different for different biasing conditions.

In our analysis we have assumed that there are—in principle—two possible sources for the low-frequency noise, resistance fluctuators, or charge fluctuators. The physical nature of the resistance fluctuators is not well understood but they can be related to charge fluctuations. For instance, a charge oscillating in the tunnel barrier may modify both the transparency and the induced island charge.

The noise from a resistance fluctuator in one of the tunnel barriers would have an asymmetry along the onset of the SET open state as it was shown in Sec. II [see Fig. 1(b)]. In order to explain the bias dependence of the cut-off frequency [see Fig. 4(a)] in terms of resistance fluctuators, we must assume that there is an individual resistance fluctuator located in each of the SET tunnel barriers. Furthermore these fluctuators must have the same tunneling rates. With this strong assumption, however, it is impossible to explain the sharp drop of the experimentally measured gate dependence of the cut-off frequency [see Fig. 4(b)].

Thus, in order to explain the results for the high-frequency Lorentzian, we will assume that there are individual charge fluctuators affecting the SET and that each Lorentzian in the experimentally measured spectra is due to a single fluctuator coupled to the SET island. Many experimental groups have suggested a microscopic nature of these fluctuators. The microscopic nature is not known well but there are suggestions that it could be traps in the substrate dielectric close to the SET or in the aluminum surface oxide.

Here we will argue that the sources of these two level fluctuators are located outside the barrier and that they may have a *mesoscopic* nature. In Ref. 26 it is argued, based on electrostatic analysis of the tunnel barrier, that such fluctuators could not be localized inside barrier. There are also other experiments,[32,33] where it is argued that the charge fluctuators (most probably) are localized outside the tunnel barrier.

A typical SET is made from thin aluminum films, which are not uniform; they consist of small grains connected to each other. In Fig. 5(a) we show a scanning electron microscopy (SEM) image of a sister sample to the measured one. In Fig. 5(b) we also show an atomic force microscopy (AFM) image of the same sister sample. It can be clearly seen that there are many small grains close to the device. We will assume that some grains are separated from the main film by a thin oxide layer but also capacitively connected to the SET island.

Electrostatically such a grain can be described as a single-electron box (SEB),[34] capacitively coupled to the SET island with capacitance C_g' and having a tunnel contact with resistance R' and capacitance C' with one of the bias leads as

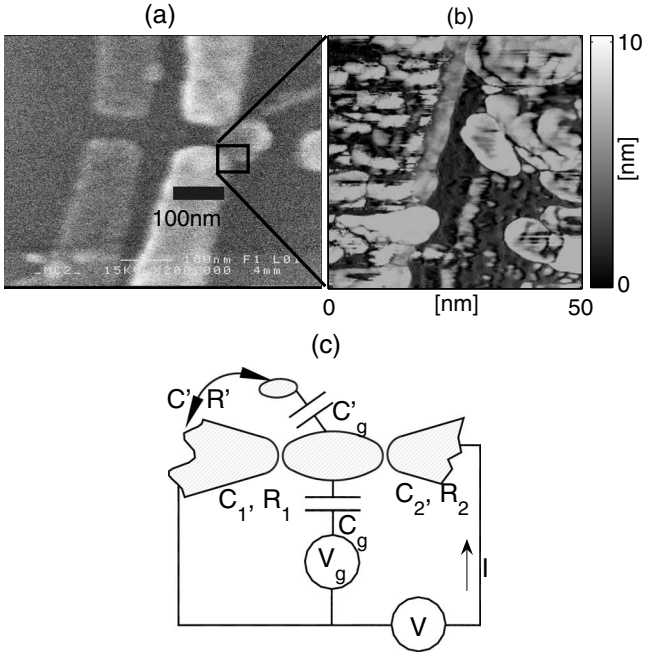

FIG. 5. (a) A SEM image of a sister sample to the measured one. The black bar shows 100 nm linear scale. (b) An AFM pictures of the edge of an aluminum film on the SiOx surface. (c) Equivalent electrostatic scheme, where the small metallic grain is capacitively coupled to the SET island and has a tunnel connection with a bias lead.

indicated in Fig. 5(c). The situation is almost equivalent if the grain would be tunnel connected to the SET island and capacitively connected to the SET-bias lead. For a detailed analysis we should estimate the energy scales for this grain. We assume that the linear dimension of the stray aluminum grain is in the range 1–5 nm. The charging energy for this grain is of the order $E'_C \equiv e^2/(2C'_\Sigma) \sim 10^{-1}$ eV, where $C'_\Sigma = C' + C'_g + C'_{\mathrm{env}}$, and C'_{env} is the capacitance to the rest of the environment. This charging energy is substantially larger than the experimental temperature and the charging energy of the SET ($k_BT \ll E_C \ll E'_C$). In addition, there will be further separation of the energy levels due to the small size of the grains.

The ratio of capacitances C'_g/C'_Σ is given directly by the charge induced in the SET island, which we already have extracted by integrating the Lorentzians. Thus for the high-frequency Lorentzian, we have $C'_g/C'_\Sigma = 0.030$ and for the low-frequency Lorentzian this ratio is 0.0066.

In our model the single-electron box is capacitively coupled to the SET island and tunnel coupled with one of the SET leads. The average potential of the SET island ϕ acts, in this system, as a gate potential for the single-electron box and induces the charge $n'_g = C'_g\phi/e$ on the grain. The charging dynamics for the electron box can be described by the orthodox theory using a master-equation approach.[30] Electron tunneling changes the number of excess electrons n in the grain. The differences in the electrostatic energy, when electrons tunnel to (+) or from (−), the grain are

$$\Delta\mathcal{E}_c^{\pm}(n) = 2E'_C(\pm n \mp n'_g + 1/2). \tag{2}$$

The tunnel rates of electron tunneling to or from the grain is a function of the tunnel resistance R' and the electrostatic energy gain $\Delta\mathcal{E}_c^{\pm}(n)$,

$$w_n^{\pm} = \frac{1}{e^2R'}\frac{\Delta\mathcal{E}_c^{\pm}(n)}{1-\exp[-\Delta\mathcal{E}_c^{\pm}(n)/(k_BT)]}. \tag{3}$$

The probability σ_n to have n excess electrons in the grain obeys the master equation,

$$\frac{d\sigma_n}{dt} = w_{n-1}^{+}\sigma_{n-1} + w_{n+1}^{-}\sigma_{n+1} - \sigma_n(w_n^{+} + w_n^{-}). \tag{4}$$

For our case of low temperature $k_BT \ll E'_C$, there are only two nonvanishing probabilities σ_n and σ_{n+1}. This simplifies the problem and it is convenient to define the distance from the grain degeneracy point, i.e., the point where these two nonvanishing states are degenerate, as $\Delta n'_g = C'_g(\phi - \phi_0)/e$. Here $\phi_0 = e(n+1/2)/C'_g$ is the SET island potential needed to reach the grain degeneracy point.

In the time domain, the dynamics for charging this grain from the lead is a random telegraph process and the spectrum of this process is a Lorentzian function with a cut-off frequency defined by the sum of charging and escaping rates,[35]

$$f_{\mathrm{co}} = w_n^{+} + w_{n+1}^{-} = \frac{\Delta n'_g}{R'C'_\Sigma}\coth\left(\frac{E'_C}{k_BT}\Delta n'_g\right)$$
$$= \mathcal{A}(\phi - \phi_0)\coth[\mathcal{B}(\phi - \phi_0)], \tag{5}$$

where $\mathcal{A} = C'_g/(eC'_\Sigma R')$ and $\mathcal{B} = eC'_g/(2k_BTC'_\Sigma)$.

From Eq. (5) we thus see that the cut-off frequency of the Lorentzian depends directly on $\Delta n'_g$ and therefore on the potential of the SET island ϕ. When the grain is biased away from its degeneracy point, i.e., when $\Delta n'_g > 2k_BT/E'_C$, the cut-off frequency grows linearly with the SET island potential. This means that if we are far from the grain degeneracy point, the cut-off frequency is relatively high and the relative frequency shift, due to the change in ϕ, will be small. On the other hand, if we are close to the grain degeneracy point, the cut-off frequency will be close to its minimum and the relative change in frequency due to ϕ can be substantial. The maximum relative frequency change occurs when the potential just barely reaches the grain degeneracy point and can be calculated from Eq. (5). Taking in to account the bounds of the island potential $-e/(2C_\Sigma) < \phi < e/(2C_\Sigma)$, we get

$$\left.\frac{\Delta f_{\mathrm{co}}}{f_{\mathrm{co,min}}}\right|_{\mathrm{max}} = \mathcal{B}\Delta\phi_{\mathrm{max}}\coth(\mathcal{B}\Delta\phi_{\mathrm{max}}) - 1$$
$$= \frac{C'_g}{C'_\Sigma}\frac{E_C}{k_BT}\coth\left(\frac{C'_g}{C'_\Sigma}\frac{E_C}{k_BT}\right) - 1. \tag{6}$$

We note that the relative frequency shift is independent of R' and that a large charging energy of the SET is important to observe a frequency shift. Thus it is clear that the relative frequency shift of most Lorentzians will be very small. To observe a frequency shift as large as in Fig. 4, the grain will have to be close to its degeneracy point and, in addition, the charging energy of the SET will have to be large to create a

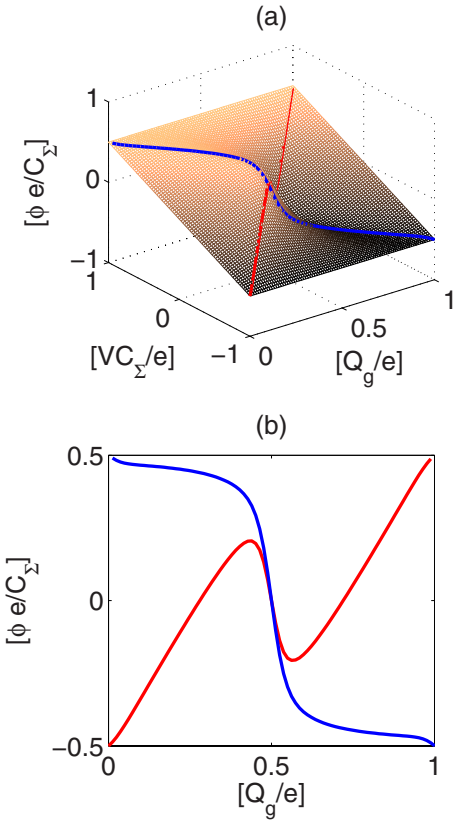

FIG. 6. (Color online) (a) The SET island potential ϕ calculated from the orthodox theory as a function of bias voltage and gate charge. (b) Line cuts along the two diagonals in (a) where the measurements have been performed. As can be seen, the potential is asymmetric with respect to the SET degeneracy point. If the grain SEB is biased away from its degeneracy point, the frequency of the tunneling on and off the grain should be proportional to the island potential. The resulting fit is shown in Fig. 7.

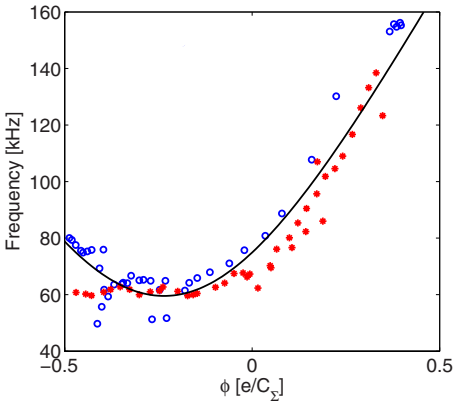

FIG. 7. (Color online) The cut-off frequency of the high-frequency Lorentzian versus the potential for the SET island. The potential is calculated from the orthodox theory for the bias and gate voltages at which the spectrum was recorded. Stars (red) represent measurements taken at positive gain (D points) whereas circles (blue) represent measurements taken at negative slopes (B points). The line is a fit to Eq. (5).

substantial frequency shift. Obviously, a relatively strong coupling between the grain and the SET island is also important.

The average potential of the SET island will depend both on the bias and gate voltages of the SET $\phi(V, V_g)$ and can be calculated using the orthodox theory.[30] We have calculated the potential as a function of bias and gate voltages as is shown in Fig. 6(a) and, in particular, we have calculated the potential along the two diagonals (roughly where the measurements have been performed), which is shown in Fig. 6(b), to give an idea of how the potential varies [cf. Figs. 1 and 2(a)]. As can be seen, the potential is asymmetric with respect to the SET degeneracy point and varies between $-e/(2C_\Sigma)$ and $e/(2C_\Sigma)$.

Inserting the calculated potential into Eq. (5), we can thus make a quantitative comparison between our model and the measured data. In Fig. 7 we plot the cut-off frequency of the high-frequency Lorentzian as a function of the SET island potential. As can be seen there is a good agreement between the data and our model (Eq. (5)). To obtain this we have used three fitting parameters, namely $\mathcal{A}$, $\mathcal{B}$, and ϕ_0 of Eq. (5). From this fit we can extract important parameters of the grain SEB. From the $\mathcal{A}$ parameter, we get the tunnel resistance to the grain using the capacitance ratio extracted from the integrated charge change of the Lorentzian Δq_{hf}. The extracted tunnel resistance is $R' = 2.4$ GΩ. Considering the size of the grain and that the sample was exposed to air before the measurement, this is quite reasonable. From the $\mathcal{B}$ parameter we can extract the temperature of the electrons in the lead $T_{\mathrm{lead}} = 130$ mK. The experiment is performed at a mixing chamber temperature of 25 mK; however, we also have to take into account that SETs are always substantially overheated above the cryostat base temperature.[22] Typically the overheating of a SET island is a few hundred millidegrees Kelvin. The lead next to the island will be colder, which is consistent with the temperature we extract. We can also see from the fit that the potential of the SET island passes through $\phi_0 = 0.22$ where the grain is at its degeneracy point.

From the above discussion, we can now also consider the low-frequency Lorentzian and try to understand why its cut-off frequency is not changing with bias or gate voltages. As can be seen in Figs. 4(c) and 4(d) we do not observe any significant change with the island potential. Assuming that the low-frequency Lorentzian is also due to a grain, then this fluctuator must be far from its grain degeneracy point and, therefore, the relative frequency change is very small. In this case the tunnel resistance to this grain must be substantially higher than that of the grain responsible for the high-frequency Lorentzian.

If we consider a large ensemble of many grains close to the tunnel junctions of a SET, most of them will only be weakly coupled to the island and will thus together make up a $1/f$ background in the noise spectrum. A few of the grains may be more strongly coupled to the island and will show up as individual Lorentzians in the noise spectrum just as we and many others have observed. In general it will be relatively rare that a strongly coupled grain is close to its degeneracy point, since the charging energy of the grain is much larger than that of the SET. In addition, we do need a large charging energy of the SET in order to change the frequency

of the fluctuator. Thus it will be quite rare that a Lorentzian will show the large change in the cut-off frequency, which we have observed. Therefore it is not so surprising that we have not been able to find this type of behavior in more samples in spite of numerous efforts.

The results presented here does not exclude that there are also other types of fluctuators with different physical mechanisms that contribute to the noise; however, we are confident that this is one type of fluctuator which we have been able to identify and found a good way to characterize.

VI. CONCLUSION

In conclusion we have measured the noise of a single-electron transistor from a few hertz up to 10 MHz. We find a spectrum with two Lorentzians superimposed on a $1/f$ background. The cut-off frequency of one of the Lorentzians depends strongly on the bias and gate voltages, whereas, the other does not. Our data is consistent with a model where the low-frequency noise comes from the random charge process of two effective single-electron boxes coupled to the SET. We suggest that these single-electron boxes are due to small aluminum grains coupled by tunneling to one of the leads and capacitively to the SET island. We are able to fit our data to this model with good agreement and we can extract parameters for one of the fluctuators.

ACKNOWLEDGMENTS

The samples were fabricated in the MC2 clean room. This work was supported by the Swedish VR and SSF and by the Wallenberg foundation.

*Present address: Low Temperature Laboratory, Helsinki University of Technology, P. O. Box 3500, 02015 TKK, Finland. Email address: sergey.kafanov@ltl.tkk.fi

[1] T. A. Fulton and G. J. Dolan, Phys. Rev. Lett. **59**, 109 (1987).
[2] K. K. Likharev, IEEE Trans. Magn. **23**, 1142 (1987).
[3] A. Aassime, D. Gunnarsson, K. Bladh, P. Delsing, and R. J. Schoelkopf, Appl. Phys. Lett. **79**, 4031 (2001).
[4] H. Brenning, S. Kafanov, T. Duty, S. Kubatkin, and P. Delsing, J. Appl. Phys. **100**, 114321 (2006).
[5] M. D. LaHaye, O. Buu, B. Camarota, and K. C. Schwab, Science **304**, 74 (2004).
[6] J. Bylander, T. Duty, and P. Delsing, Nature (London) **434**, 361 (2005).
[7] W. Lu, Z. Ji, L. Pfeiffer, K. W. West, and A. J. Rimberg, Nature (London) **423**, 422 (2003).
[8] T. Duty, D. Gunnarsson, K. Bladh, and P. Delsing, Phys. Rev. B **69**, 140503(R) (2004).
[9] K. W. Lehnert, K. Bladh, L. F. Spietz, D. Gunnarsson, D. I. Schuster, P. Delsing, and R. J. Schoelkopf, Phys. Rev. Lett. **90**, 027002 (2003).
[10] Yu. A. Pashkin, T. Yamamoto, O. Astafiev, Y. Nakamura, D. V. Averin, and J. S. Tsai, Nature (London) **421**, 823 (2003).
[11] M. H. Devoret and R. J. Schoelkopf, Nature (London) **406**, 1039 (2000).
[12] A. N. Korotkov, D. V. Averin, K. K. Likharev, and S. A. Vasenko, *Single Electron Tunneling and Mesoscopic Devices* (Springer, New York, 1992), p. 45.
[13] H. Birk, M. J. M. de Jong, and C. Schönenberger, Phys. Rev. Lett. **75**, 1610 (1995).
[14] D. Song, A. Amar, C. J. Lobb, and F. C. Wellstood, IEEE Trans. Appl. Supercond. **5**, 3085 (1995).
[15] G. Zimmerli, T. M. Eiles, R. L. Kautz, and J. M. Martinis, Appl. Phys. Lett. **61**, 237 (1992).
[16] G. Ithier, E. Collin, P. Joyez, P. J. Meeson, D. Vion, D. Esteve, F. Chiarello, A. Shnirman, Y. Makhlin, J. Schriefl, and G. Schon, Phys. Rev. B **72**, 134519 (2005).
[17] V. Bouchiat, Ph.D. thesis, Université de Paris 6, 1997.
[18] M. Kenyon, J. L. Cobb, A. Amar, D. Song, N. M. Zimmerman, C. J. Lobb, and F. C. Wellstood, J. Low Temp. Phys. **123**, 103 (2001).
[19] V. A. Krupenin, D. E. Presnov, M. N. Savvateev, H. Scherer, A. B. Zorin, and J. Niemeyer, J. Appl. Phys. **84**, 3212 (1998).
[20] B. Starmark, T. Henning, T. Claeson, P. Delsing, and A. N. Korotkov, J. Appl. Phys. **86**, 2132 (1999).
[21] A. N. Tavkhelidze and J. Mygind, J. Appl. Phys. **83**, 310 (1998).
[22] S. M. Verbrugh, M. L. Benhamadi, E. H. Visscher, and J. E. Mooij, J. Appl. Phys. **78**, 2830 (1995).
[23] H. Wolf, F. J. Ahlers, J. Niemeyer, H. Scherer, T. Weimann, A. B. Zorin, V. A. Krupenin, S. V. Lotkhov, and D. E. Presnov, IEEE Trans. Instrum. Meas. **46**, 303 (1997).
[24] N. M. Zimmerman, J. L. Cobb, and A. F. Clark, Phys. Rev. B **56**, 7675 (1997).
[25] T. F. Li, Yu. A. Pashkin, O. Astafiev, Y. Nakamura, J. S. Tsai, and H. Im, Appl. Phys. Lett. **91**, 033107 (2007).
[26] A. B. Zorin, F. J. Ahlers, J. Niemeyer, T. Weimann, H. Wolf, V. A. Krupenin, and S. V. Lotkhov, Phys. Rev. B **53**, 13682 (1996).
[27] R. J. Schoelkopf, P. Wahlgren, A. A. Kozhevnikov, P. Delsing, and D. E. Prober, Science **280**, 1238 (1998).
[28] P. Wahlgren, Ph.D. thesis, Chalmers University of Technology, 1998.
[29] A. N. Korotkov (unpublished).
[30] D. V. Averin and K. K. Likharev, *Mesoscopic Phenomena on Solids* (North-Holland, Amsterdam, 1991), p. 173.
[31] K. Segall, K. W. Lehnert, T. R. Stevenson, R. J. Schoelkopf, P. Wahlgren, A. Aassime, and P. Delsing, Appl. Phys. Lett. **81**, 4859 (2002).
[32] T. M. Buehler, D. J. Reilly, R. P. Starrett, V. C. Chan, A. R. Hamilton, A. S. Dzurak, and R. G. Clark, J. Appl. Phys. **96**, 6827 (2004).
[33] M. Furlan and S. V. Lotkhov, Phys. Rev. B **67**, 205313 (2003).
[34] P. Lafarge, H. Pothier, E. R. Williams, D. Esteve, C. Urbina, and M. H. Devoret, Z. Phys. B: Condens. Matter **85**, 327 (1991).
[35] S. Machlup, J. Appl. Phys. **25**, 341 (1954).